Applied Catalysis B: Environmental 204 (2017) 385–393

Contents lists available at ScienceDirect

Applied Catalysis B: Environmental

journal homepage: www.elsevier.com/locate/apcatb

Novel AuPd bimetallic alloy decorated 2D $BiVO_4$ nanosheets with enhanced photocatalytic performance under visible light irradiation

Junlong Zhang[a,b], Yan Lu[b], Lei Ge[a,b,*], Changcun Han[b], Yujing Li[b], Yangqin Gao[b], Songsong Li[b], Hao Xu[b]

[a] State Key Laboratory of Heavy Oil Processing, College of Science, China University of Petroleum Beijing, No. 18 Fuxue Rd., Beijing 102249, People's Republic of China

[b] Department of Materials Science and Engineering, College of Science, China University of Petroleum Beijing, No. 18 Fuxue Rd., Beijing 102249, People's Republic of China

ARTICLE INFO

Article history:
Received 18 September 2016
Received in revised form
24 November 2016
Accepted 25 November 2016
Available online 25 November 2016

Keywords:
2D $BiVO_4$ nanosheets
AuPd bimetallic alloy
Rhodamine B
Composite photocatalysts
Photocatalysis

ABSTRACT

Novel AuPd bimetallic alloy nanoparticles (NPs) decorated two-dimensional (2D) $BiVO_4$ nanosheet photocatalysts were successfully synthesized via mild wet-chemical process and facile deposition procedure. The composite photocatalysts were characterized by X-ray diffraction (XRD), scanning electron microscopy (SEM), transmission electronic microscope (TEM), X-ray photoelectron spectroscopy (XPS), UV–vis diffuse reflection spectroscopy (DRS), electron spin resonance (ESR) and surface photovoltage spectroscopy (SPV). The 1.0 wt% AuPd/$BiVO_4$ nanosheets showed highest photocatalytic activity for the degradation of Rhodamine B (RhB) under visible light (300 W Xe lamp coupled with a UV-cutoff filter ($\lambda \geq 400$ nm)), and the photocatalytic efficiency was improved for about 21.9 and 6.1 times as compared to that of pure $BiVO_4$ and 1.0 wt% Au/$BiVO_4$, respectively. The novel AuPd/$BiVO_4$ composites may make a way to synthesize 2D semiconductor composites with potential applications for solar energy conversion and environmental purifications.

1. Introduction

In the past few years, tremendous interest has been attracted by researchers related to photocatalytic pollutant degradation and water splitting, in which an ideal "green" technology known as semiconductor photocatalysis plays a vital role [1–4]. To develop more efficient photocatalysts with reasonable photocatalytic activities for practical applications, photocatalyst exhibits photocatalytic activity in visible range is required and so called "visible-light-active photocatalyst", such as $BiVO_4$ [5,6], Bi_2WO_6 [7], AgX(AgCl, AgBr) [8,9], C_3N_4 [10] and CdS [11] have been developed and investigated as promising candidates to replace traditional non-visible-active photocatalysts, such as TiO_2. With their intrinsic advantage to utilize solar energy covering the visible range, the research on visible-light-active photocatalysts with high stability is becoming more important with time.

Recently, $BiVO_4$ has attracted much attention, which due to not only its potential application in photocatalytic water oxidation and degradation of hazardous organic pollutants, but also its good chemical stsbility under visible light irradiation [12,13]. It has been shown that the photocatalytic activity of $BiVO_4$ depends strongly on its crystalline forms as well as microstructures. Generally, $BiVO_4$ has three crystalline phases [14], among which the monoclinic scheelite $BiVO_4$ (m-$BiVO_4$) has a band gap of 2.4–2.5 eV and shows much higher photocatalytic activity than the other two forms. m-$BiVO_4$ could be prepared into multifarious morphologies, such as nanosheets [5], nanoribbons [15], decahedrons [16], spheres [17], and hollow structure in olive shape [18]. Among them, we select two-dimensional nanosheets (m-$BiVO_4$) as a support due to their large surface areas and quantum confinement effect arises from its thin sheet thickness in several nanometers.

Besides of playing with the crystalline forms and microstructures, constructing composite structures is also proven to be an effective method to enhance the photocatalytic performance of m-$BiVO_4$, especially when considering the low separation efficiency of electron-hole pairs present in pristine m-$BiVO_4$. Much effort has been spent to address the problem of low charge separation efficiency, such as combining m-$BiVO_4$ with metals [6,19,20], metal oxides [21,22], carbon materials [23] and silver compounds

* Corresponding author at: State Key Laboratory of Heavy Oil Processing, China University of Petroleum Beijing, No. 18 Fuxue Road, Beijing, 102249, People's Republic of China.
E-mail address: gelei@cup.edu.cn (L. Ge).

http://dx.doi.org/10.1016/j.apcatb.2016.11.057
0926-3373/

which showed improved photocatalytic performance, but is still under investigation for further improvement [24]. Metal nanoparticles, especially noble metals, such as Au, Ag, Pd and Pt, are studied as wonderful co-catalyst for photocatalysis. The low lying of Fermi levels in noble metals provide additional benefits for prolonging the lifetime of charge carriers to further improve the photocatalytic activity. Meanwhile, various bimetallic alloy NPs have been reported, such as AuPd [25], AuAg [26], PtCo [27] and PtCu [28] and exhibit superior activity than their corresponding monometallic NPs. Among them, AuPd NPs have been studied in multiple domains, including selective oxidation of primary carbon-hydrogen bonds [29], photocatalytic hydrogen evolution [30], electrocatalyst for ethanol oxidation [31] and phenol photodecomposition [32]. Although there are some literatures have reported the photocatalytic performance of m-$BiVO_4$ and AuPd alloy respectively, but the RhB degradation performance of the AuPd/$BiVO_4$ composite which the AuPd NPs may be a promising candidate to construct composite structures with m-$BiVO_4$ to exhibit enhanced photocatalytic performance was not reported.

In this study, for the first time we proposed a facile method to prepare novel AuPd/$BiVO_4$ composites by in-situ depositing AuPd NPs on the surface of 2D m-$BiVO_4$ nanosheets. The photocatalytic activity was investigated by degradation of Rhodamine B (RhB) under visible light irradiation and reconfirmed with degradation of phenol. The result indicated that the as-prepared AuPd/$BiVO_4$ nanosheets showed significantly enhanced photocatalytic activities than pure $BiVO_4$. The active photocatalytic species and dynamic behavior of photo-generated charge carriers were investigated via ESR and SPV techniques. A possible photocatalytic mechanism was proposed to illustrate the separation and transfer behaviors of photo-generated electron-hole pairs in the AuPd/$BiVO_4$. The successful development of the novel AuPd/$BiVO_4$ nanosheets with enhanced photocatalytic activity and acceptable stability may pave a way to synthesize 2D semiconductor composites for potential applications in light energy conversion and environmental purification.

2. Experimental

2.1. Materials

Bismuth nitrate pentahydrate ($Bi(NO_3)_3{\cdot}5H_2O$, Aladdin, 98% A.C.S), ammonium metavanadate (NH_4VO_3, A.R.), sodium dodecylbenzenesulfonate ($C_{18}H_{29}NaO_3S$, A.R.), sodium hydroxide (NaOH, A.R.), nitric acid (HNO_3, 65%), Sodium borohydride ($NaBH_4$, Aladdin, 98%), poly vinyl alcohol (PVA, Aldrich, MW = 10 000, 80% hydrolyzed), ethyl alcohol (EtOH, A.R.) and Rhodamine B (RhB, A.R.) were used as purchased without further purification. Deionized water was used as the solvent for all of the solutions or dispersions.

2.2. Synthesis of the $BiVO_4$ nanosheets

The $BiVO_4$ nanosheets were prepared according to reference [5] with slight modification. In a typical procedure, 1 mmol $Bi(NO_3)_3{\cdot}5H_2O$ and 0.72 mmol $C_{18}H_{29}NaO_3S$ (SDBS) were initially dissolved in 10.0 mL 4.0 mol/L HNO_3 solution and the resultant solution was marked as solution A. Simultaneously, 1.0 mmol NH_4VO_3 was added into 10.0 mL 2.0 mol/L NaOH solution, and the resultant solution was marked as solution B. Then, solution B was added into solution A under vigorous stirring. The pH of the mixed solution was adjusted to 6.5 with 2 M NaOH solution. The resultant solution was sealed in Teflon-lined stainless steel autoclave which was heated at 160 °C for 3 h. The precipitate (vivid yellow) was collected by centrifugation and rinsed with distilled water and absolute alcohol and then dried at 100 °C for 4 h.

2.3. Synthesis of AuPd/$BiVO_4$

The AuPd alloy NPs were prepared as follow [25,33]: 10 mM $HAuCl_4{\cdot}3H_2O$ and $PdCl_2$ aqueous solution were prepared as stock solutions. Fresh aqueous solutions of 0.1 M $NaBH_4$ and 1.0 wt% poly vinyl alcohol (PVA) were also prepared. The prepared $BiVO_4$ nanosheets (0.1 g) were dispersed in 50 mL deionized water to form homogeneous suspension under continuous stirring. Then the $PdCl_2$ and $HAuCl_4{\cdot}3H_2O$ stock solution was mixed in desired ratio (Au/Pd = 1, weight ratio) and an appropriate amount of PVA solution was added (PVA/(Au + Pd) = 1.2, weight ratio). After that, the fresh $NaBH_4$ solution ($NaBH_4$/(Au + Pd) = 5, molar ratio) was added and a dark green solution was obtained. After stirring for 2 h at room temperature, the products were purified and collected, then dried at 80 °C. With the same procedure, AuPd/$BiVO_4$ with different weight ratio of AuPd bimetallic NPs was obtained by changing the weight contents of AuPd precursors in the mixed solution. 1.0 wt% Au/$BiVO_4$ and 1.0 wt% Pd/$BiVO_4$ was also synthesized for comparison by using the same procedure with pure Au or Pd precursors.

2.4. Characterization

The crystal structure of the samples was analyzed by X-ray diffraction (XRD; Bruker D8 Advance, X-ray diffractometer) with CuKα radiation at a scan step size of 3°. The morphology of the samples was examined by field emission canning electronic microscope (FESEM, FEI Quanta 200F) and high resolution transmission electron microscopy (HRTEM). UV–vis diffuse reflection spectroscopy (DRS) was performed on a Shimadzu UV-4100 spectrophotometer using $BaSO_4$ as the reference material. The X-ray photoelectron spectroscopy (XPS) was measured on a PHI 5300 ESCA system with a beam voltage of 3.0 eV, and the energy of Ar ion beam was 1.0 keV to detect the composition of the final products. The binding energies were normalized to the signal for adventitious carbon at 284.8 eV. The electron spin resonance (ESR) signals of spin-trapped oxidative radicals were obtained on a Bruker model ESR JES-FA200 spectrometer equipped with a quanta-Ray Nd:YAG laser system as the light source, in which a UV-cutoff filter ($\lambda \geq 400$ nm) was used.

2.5. SPV measurements

The surface photovoltage (SPV) measurement was carried out on a surface photovoltage spectroscopy (PL-SPS/IPCE1000 Beijing Perfect Light Technology Co., Ltd). The measurement system consists of a source of monochromatic light, a locking amplifier (SR830, Stanford research systems, Inc.) with a light chopper (SR540, Stanford research systems, Inc.), and a simple chamber. The monochromatic light is provided by passing light from a 500 W xenon lamp (CHFXQ500 W, global xenon lamp power) though a grating monochromator (Omni-5007, No.09010, Zolix), which chopped with a frequency of 24 Hz. All the measurements were operated under ambient pressure at room temperature.

2.6. Photocatalytic activity

The photocatalytic activities of the as-prepared samples were investigated by degradation of RhB under visible-light irradiation. In a typical photocatalytic experiment, 0.05 g photocatalyst powder was suspended in 100 mL RhB aqueous solution (10 mg/L). The suspension was stirred in the dark for 1 h to establish adsorption-desorption equilibrium. After that, 300 W Xe lamp coupled with a UV-cutoff filter ($\lambda \geq 400$ nm) was used as the visible light source to irradiate the suspensions under vigorous stirring. The light intensity employed was 72 mW cm^{-2}. After irradiation, 4 mL sample solution was collected at certain time interval, the photocatalysts were removed by centrifugation, and the remaining solution was

analyzed by the absorption of RhB at 552 nm using UV-1700 spectrometer.

The photodegradation of colorless phenol was also performed. In the phenol degradation process, 50 mg photocatalyst powder was suspended in 100 mL phenol solution (20 mg/L), other steps are the same as RhB degradation process. The solution was collected in certain intervals and centrifuged, and phenol absorption in the collected liquid was then analyzed by UV-1700 spectrometer at 270 nm (quartz cuvette).

3. Results and discussion

3.1. Characterization of AuPd/$BiVO_4$ composites

The crystal structure and phase purity of as-prepared products were first verified by XRD analysis. The representative XRD patterns of $BiVO_4$ nanosheets and $BiVO_4$ nanosheet cocatalyzed with noble metals are shown in Fig. 1, data of the standard card of monoclinic $BiVO_4$ (JCPDS No. 14-0688) are also shown as reference. Well correlation of main peak positions can be seen as compare the $BiVO_4$ nanosheets diffraction pattern with the reference, indi-

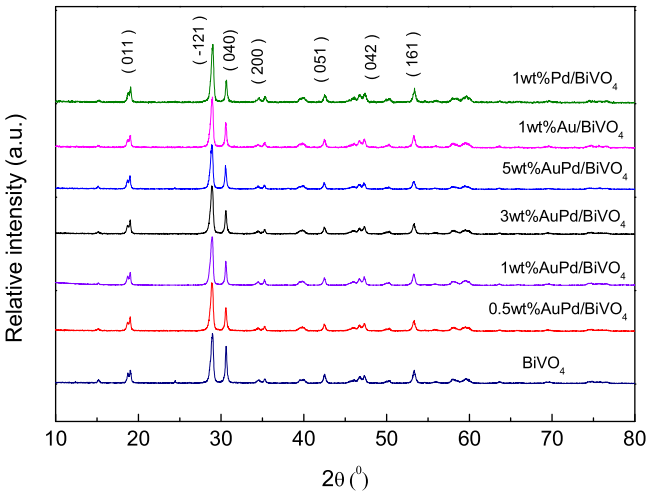

Fig 1. XRD patterns of pure $BiVO_4$ nanosheets, $Au/BiVO_4$, $Pd/BiVO_4$ and $AuPd/BiVO_4$ composites with different weight ratios of AuPd bimetallic NPs.

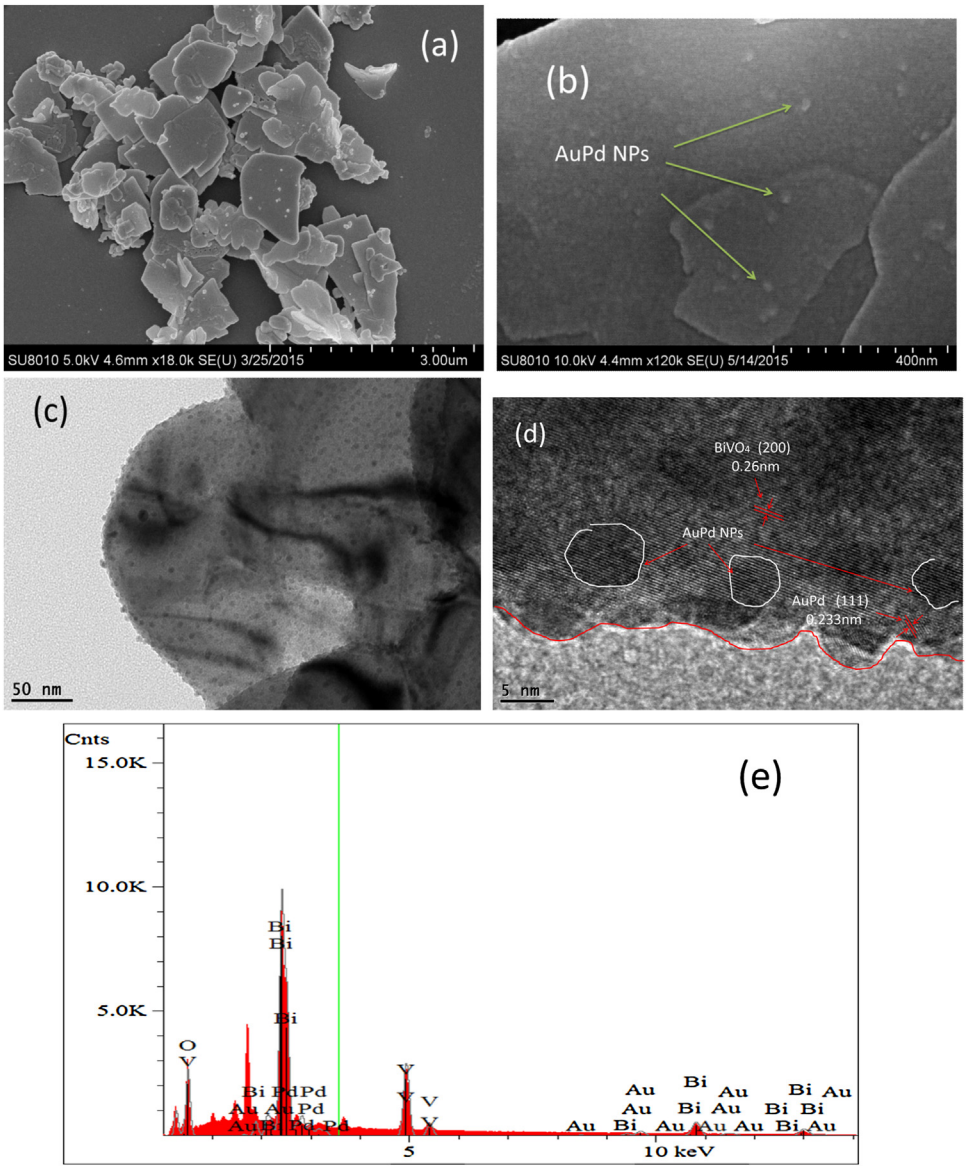

Fig. 2. SEM images of pure $BiVO_4$ (a), $AuPd/BiVO_4$ (b), TEM image (c), HRTEM image (d) and EDX spectra (e) of the $AuPd/BiVO_4$ sample.

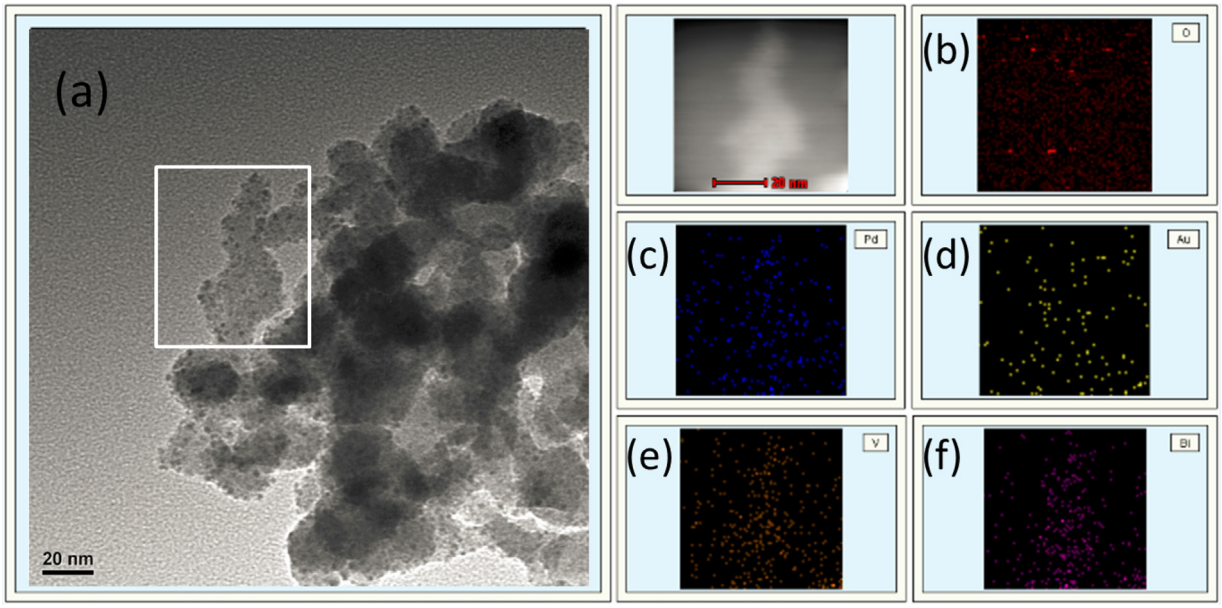

Fig. 3. TEM image of AuPd/$BiVO_4$ at low magnification (a); elemental distribution mapping of (b) O, (c) Pd, (d) Au, (e) V and (f) Bi.

cating the $BiVO_4$ nanosheets are mainly composed by monoclinic $BiVO_4$ with little impurity. The main peaks at 2θ of 18.99°, 28.82°, 30.55°, 42.46°, 47.31° and 53.31° can be readily indexed to the (011), (1$\bar{2}$1), (040), (051), (042) and (161) planes of monoclinic $BiVO_4$, respectively. Clearly, the AuPd/$BiVO_4$ composites have similar XRD patterns as the $BiVO_4$ nanosheets with indistinguishable difference, indicates the $BiVO_4$ crystal structure keeps unchanged during the reduction of noble metal precursors to metal NPs in $NaBH_4$ solution. No typical diffraction peaks of AuPd alloy can be observed in the XRD patterns for AuPd/$BiVO_4$ composites with different weight ratio of AuPd NPs, which may due to the low contents of AuPd in the AuPd/$BiVO_4$ composites.

To confirm the successful loading of AuPd NPs on the $BiVO_4$ nanosheets, elemental and microstructure morphology analysis were performed by HRTEM and SEM characterization. Fig. 2 presents typical TEM and SEM images of AuPd/$BiVO_4$ composite with X% loading of AuPd NPs. The SEM image shows the pure $BiVO_4$ sample has a well-defined nanosheet structure with smooth surface (Fig. 2a). Rough surface is shown in AuPd/$BiVO_4$ composite which small NPs loaded on the surface of $BiVO_4$ (Fig. 2b), indicating AuPd NPs are successfully loaded on the $BiVO_4$ nanosheets. A close TEM view of the AuPd/$BiVO_4$ composite (Fig. 2c) reveals the AuPd NPs are uniformly distributed on the surface of $BiVO_4$ nanosheets with an average size of ~7 nm. A representative HRTEM image which taken from a selected area of the AuPd/$BiVO_4$ composite structure is shown in Fig. 2d. The spacing of the lattice fringe is found to be about 2.33 nm can be well indexed as (111) plane of the AuPd nanoparticles, which confirms the surface loaded NPs are AuPd NPs [33]. The intimate interfaces formed between AuPd NPs and $BiVO_4$ nanosheets as viewed in HRTEM image is favorable for charge separation and transfer of charge carriers. The signal of Au and Pd shown in EDX pattern (Fig. 2e) further confirm the presence of AuPd in the composites. Fig. 3(a) shows a TEM image of AuPd/$BiVO_4$ at low magnification. Fig. 3(b–f) displays the elemental distribution maps (O, Pd, Au, V and Bi respectively) determined by energy-filtered TEM technique through the nanostructure in Fig. 3(a). The result of AuPd/$BiVO_4$ shows that elements of Bi, V, O, Au and Pd can be clearly observed. It is found that Bi, V, O, Au and Pd elements distribute almost uniformly in the surface of AuPd/$BiVO_4$, which further confirmed the AuPd/$BiVO_4$ composite photocatalysts were prepared successfully.

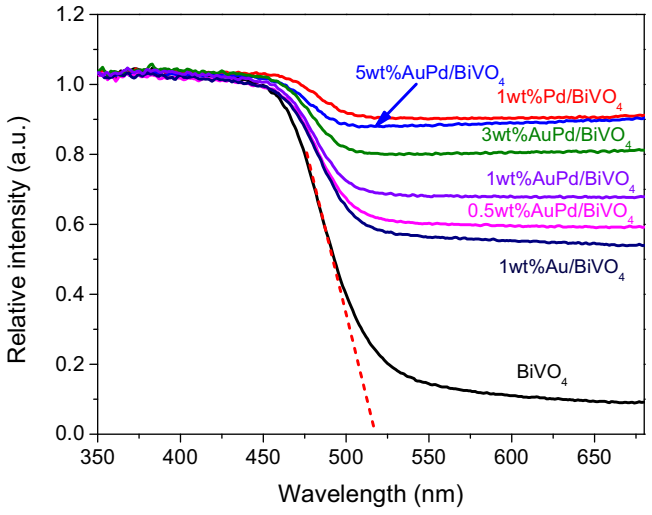

Fig. 4. UV–vis diffuse reflectance spectra of pure $BiVO_4$ nanosheets, Au/$BiVO_4$, Pd/$BiVO_4$ and AuPd/$BiVO_4$ composites with different weight ratios of AuPd NPs.

The UV–vis diffuse reflectance spectra of AuPd/$BiVO_4$ composites with different weight ratio of AuPd NPs, together with that of $BiVO_4$ nanosheets were investigated and shown in Fig. 4. The $BiVO_4$ nanosheets have absorption from the UV range up to about 517 nm in the visible range, and the red tangent line of spectrum denotes that the visible light absorption is ascribed to the band gap transition, in accordance with the reported band gap of ~2.4 eV for $BiVO_4$. With the introduction of AuPd alloy nanoparticles, the colors of AuPd/$BiVO_4$ samples are changed from yellow to dark grey. The AuPd/$BiVO_4$ composites display similar absorption edge after introduction of different weight ratio of AuPd NPs, but exhibit significantly enhanced absorption in visible range beyond the optical response of $BiVO_4$. The increase in visible light absorption with higher AuPd NPs weight ratio clearly demonstrate that the enhanced light absorption beyond the optical response of $BiVO_4$ arises from the absorption of AuPd NPs, which confirms that the introduction of AuPd NPs could improve the visible light absorption of $BiVO_4$. It is worth to note that enhanced light absorption usually accompany with improved photocatalytic performance.

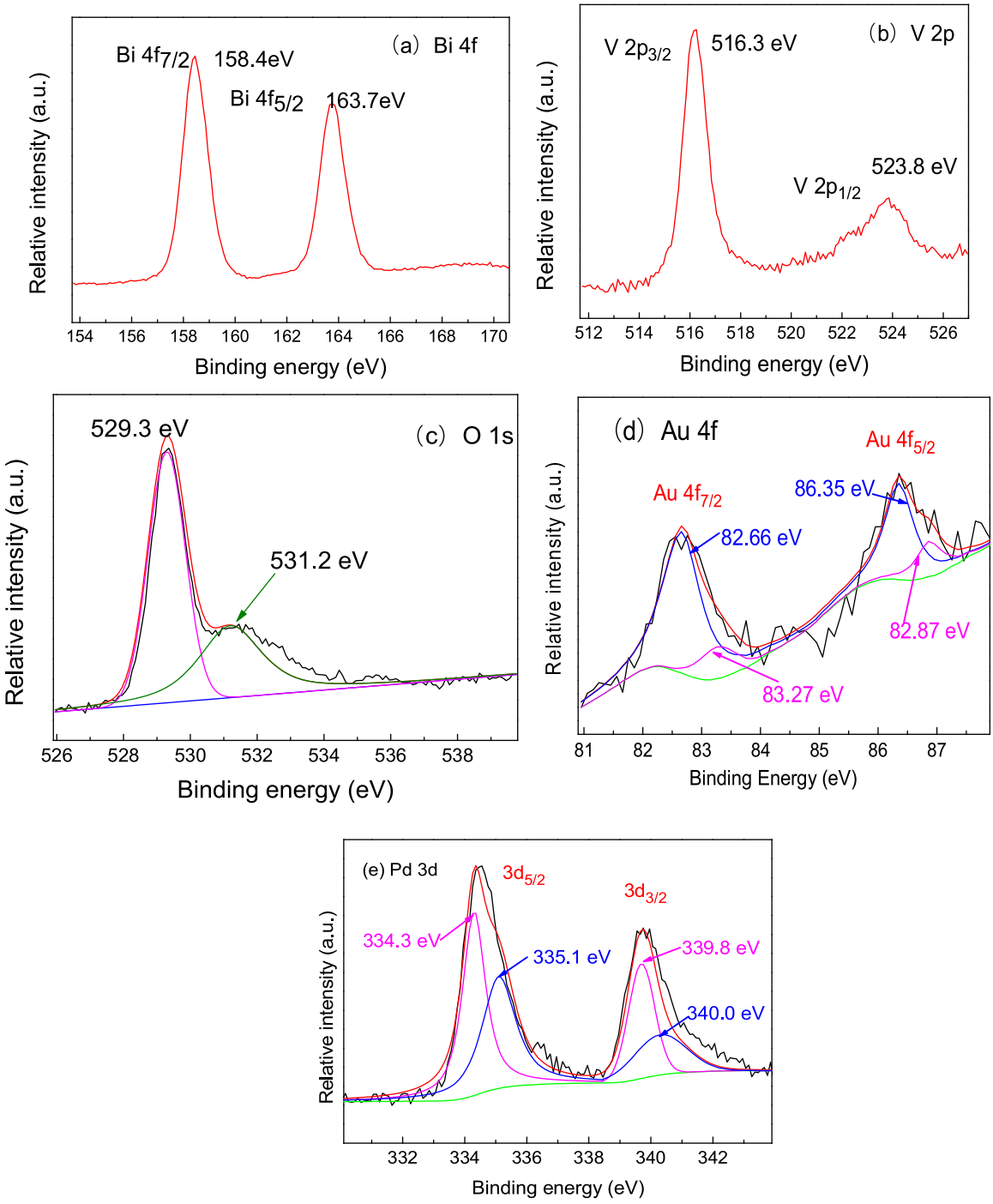

Fig. 5. XPS spectra of AuPd/$BiVO_4$ samples: (a) Bi 4f; (b) V 2p; (c) O 1s; (d) Au 4f;(e)Pd 3d.

The surface element composition and atomic valence state of AuPd/$BiVO_4$ sample with 1.0 wt% AuPd was examined by X-ray photoelectron spectroscopy (XPS). In Fig. 5a, the two peaks fitted at 158.4 and 163.7 eV are the signals of Bi $4f_{7/2}$ and Bi $4f_{5/2}$, which are less than that of 158.9 eV and 164.3 eV of pure $BiVO_4$ [34]. This phenomenon indicates that there may have an interaction on the interface between AuPd NPs and $BiVO_4$ nanosheets. The V 2p peaks located at 516.3 and 523.8 eV are in accordance with the V $2p_{3/2}$ and V $2p_{1/2}$ in the $BiVO_4$ (Fig. 5b). It can be clearly observed that O 1s spectra can be fitted into two peaks, representing the presence of different oxygen species on the sample surface, including lattice oxide (O_I) species(529.3 eV) and adsorbed oxygen (O_{II}) species(531.2 eV) in Fig. 5c [35]. The Au 4f XPS spectra (Fig. 5d) shows that two peaks at 82.66 and 86.35 eV can be assigned to $4f_{7/2}$ and $4f_{5/2}$ of Au^0 species, which exhibits slight negative shift as compared to previous report [36]. The shift may be due to the unique structure of AuPd bimetallic alloys. As shown in Fig. 5e, two asymmetric peaks which located at 334.3 and 339.8 eV are the signals of Pd $3d_{5/2}$ and Pd $3d_{3/2}$, respectively. It is attributed to the metallic Pd^0 species. However, the binding energy peak centered at 335.1 and 340.1 eV are originates from of Pd^{2+} species. The result is in accordance with our previous work [25], and may be ascribed to the charge transfer between Au and Pd in AuPd bimetallic alloy.

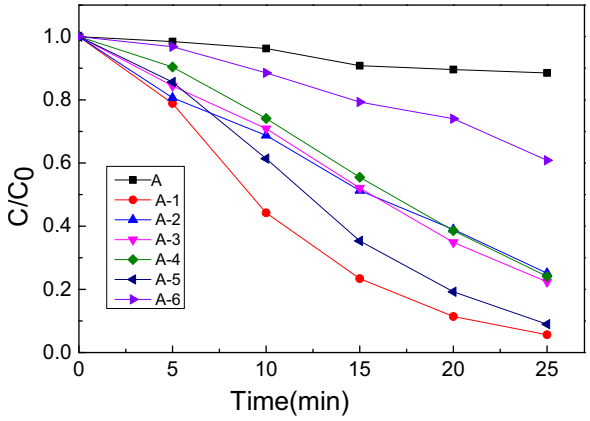

Fig. 6. The photodegradation curves of RhB over different photocatalyst: pure $BiVO_4$ (A), 1.0 wt% AuPd/$BiVO_4$ (A-1), 0.5 wt% AuPd/$BiVO_4$ (A-2), 3 wt% AuPd/$BiVO_4$ (A-3), 5.0 wt% AuPd/$BiVO_4$ (A-4), 1.0 wt% Pd/$BiVO_4$ (A-5), 1.0 wt% Au/$BiVO_4$ (A-6) under visible-light irradiation.

3.2. Visible light photocatalytic activity of AuPd/$BiVO_4$ samples

There are lots of documents studied the photoactivity of $BiVO_4$-based photocatalysts through degradation of RhB. Li et al. prepared $BiVO_4$/BiOBr composite by a simple one-pot hydrothermal process which the RhB (50 mL, 10 mg/L) was completely degraded in 15 min under the illumination of visible light ($\lambda > 420$ nm) [37]. The Z-scheme CdS/$BiVO_4$ NWs with different weight ratios were synthesized by Zhou et al., in which the 1:2 CdS/$BiVO_4$ could complete degradation of RhB (50 mL, 2×10^{-5} M) only took 35 min under visible light ($\lambda > 420$ nm) [38]. Yu et al. prepared RGO/$BiVO_4$ composite through an in-situ hydrothermal-assisted growth strategy which 10 mg/L RhB solution was completely degraded in 8 h under natural sunlight [39]. The photocatalytic activity of the as-prepared samples was studied by the degradation of RhB under visible light irradiation ($\lambda \geq 400$ nm). As compared to the as-prepared $BiVO_4$ nanosheets, all of the co-catalyzed samples with surface decoration of AuPd, Au and Pd NPs exhibit significantly enhanced photocatalytic activity (Fig. 6). Interestingly, for the samples with the same loading amount of co-catalyst, the AuPd/$BiVO_4$ sample shows higher photocatalytic activity than the samples decorated by pure Au or Pd NPs, which reveals a superior photocatalytic activity enhancement of AuPd NPs as compared to pure Au and Pd NPs. This superior photocatalytic activity enhancement for AuPd/$BiVO_4$ sample can be attributed to the formation of intimate interfaces between AuPd NPs and $BiVO_4$ nanosheets, in turns the separation efficiency of photo-excited charge carriers is effectively promoted. The photocatalytic activity of AuPd/$BiVO_4$ sample shows an increase at the initial stage with increasing the AuPd NPs weight ratio, reaching the highest point at 1 wt% loading of AuPd NPs, and then declines with further loading of AuPd NPs. This decline in photocatalytic activity with further loading of AuPd NPs can be related to the increase in the opacity of the composite samples. Furthermore, introduction of higher content of AuPd NPs would also lead to active site covering on the surface of $BiVO_4$, which hinders the migration of charge carriers at the semincoductor/electrolyte interface. These results indicate that appropriate loading of AuPd NPs on $BiVO_4$ nanosheets indeed contribute to improve the photocatalytic activity toward the degradation of organic dyes under visible light.

To further quantitatively investigate the reaction kinetics of the RhB photodegradation, the RhB photodegradation data was fitted by applying a first-order model [40]. The corresponding $\ln(C_0/C)$ plot is shown in Fig. 7a and the fitted degradation rate constant of RhB is illustrated in Fig. 7b. It is obvious that the 1.0 wt% AuPd/$BiVO_4$(A-1) sample has the maximum degradation

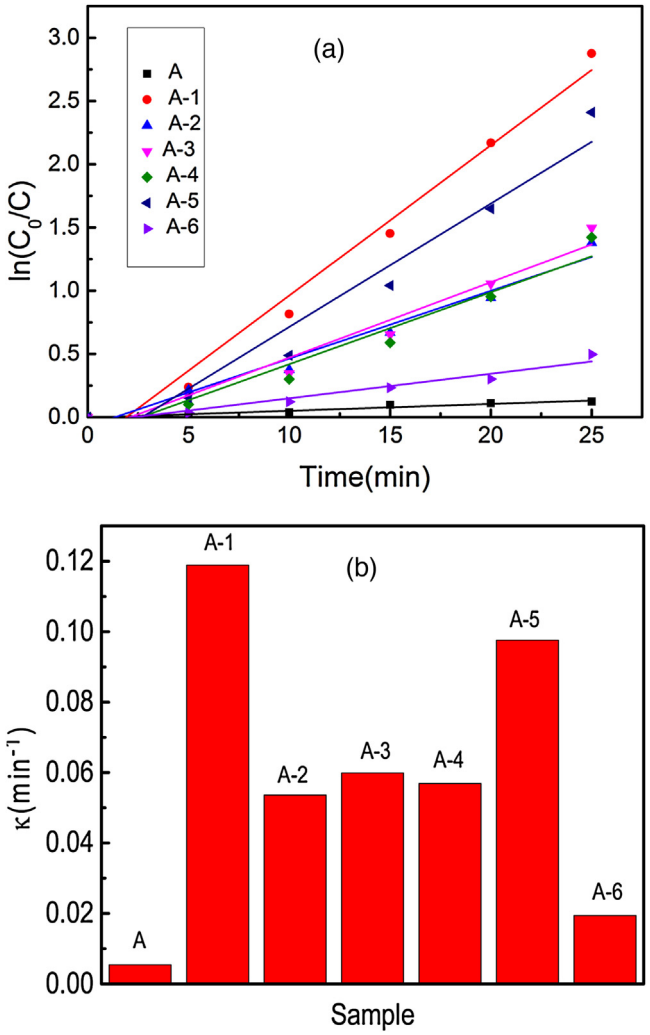

Fig. 7. (a) The first-order kinetics of RhB degradation of different photocatalyst $BiVO_4$ (A), 1 wt% AuPd/$BiVO_4$ (A-1), 0.5 wt% AuPd/$BiVO_4$ (A-2), 3.0 wt% AuPd/$BiVO_4$ (A-3), 5.0 wt% AuPd/$BiVO_4$ (A-4), 1.0 wt% Pd/$BiVO_4$ (A-5), 1.0 wt% Au/$BiVO_4$ (A-6) under visible light irradiation. (b) The degradation rate constant of RhB with different samples.

rate constant, and is about 21.9, 6.1 and 1.2 times higher than the pure $BiVO_4$(A), 1.0 wt% Au/$BiVO_4$(A-6) and 1.0 wt% Pd/$BiVO_4$(A-5), respectively. The high catalytic performance can be attributed to the formation of the intimate interfaces between AuPd NPs and $BiVO_4$ nanosheets as mentioned before, which are favorable of transfer and separation of the photo-excited charge carriers generated in $BiVO_4$.

The RhB dye photosensitization effect may exist in the reaction process, and the dye sensitization makes the photodegradation of RhB more easily. In order to eliminate the phenomenon caused by the dye sensitization, degradation of colorless organic phenol was also investigated to further verify the photocatalytic ability of 1.0 wt% AuPd/$BiVO_4$. The photodecomposition of phenol is slower than RhB, but still reached 56% degradation within 2 h under visible light irradiation (Fig. 8). The low performance for photodecomposition of phenol is due to the concentrated solution used in the experiment, which is twice higher than the one used in photodegradation of RhB, and also because the stable benzene ring exist in the phenol molecule, which is difficult to decompose. To some extent, the result confirms that the as-prepared AuPd/$BiVO_4$ has photocatalytic ability and can effectively degrade organic molecules.

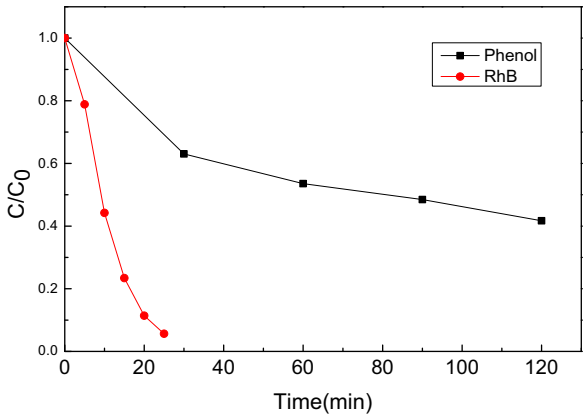

Fig. 8. The photodegradation curves (red line) of RhB dye, and the phenol photodecomposition curve (blue line) over 1.0 wt% AuPd/$BiVO_4$ sample under visible irradiation. (For interpretation of the references to colour in this figure legend, the reader is referred to the web version of this article.)

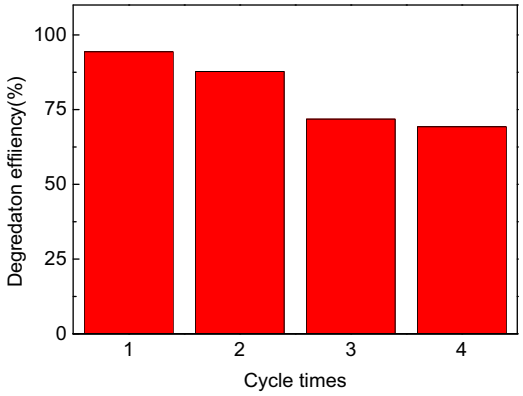

Fig. 9. Cycling runs for the photocatalytic degradation of methyl orange in the presence of 1 wt% Pd/$BiVO_4$ composite under visible light irradiation. (For interpretation of the references to colour in this figure legend, the reader is referred to the web version of this article.)

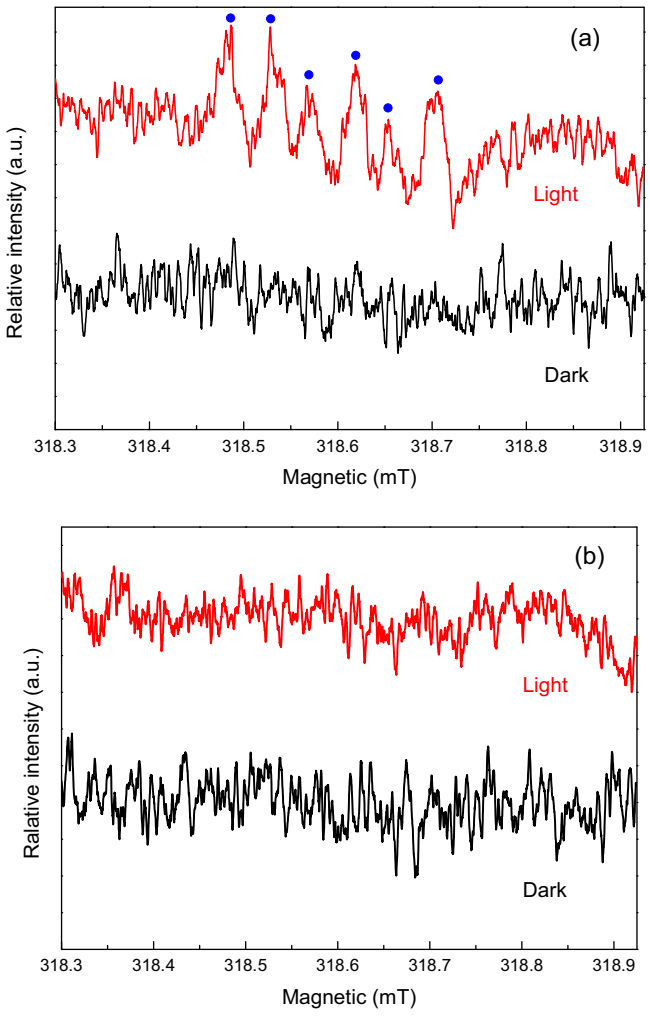

Fig. 10. ESR spectra record at ambient temperature with 1.0 wt% AuPd/$BiVO_4$ photocatalyst in: (a) methanol;(b)H_2O.

The stability of a photocatalyst is a critical attribute for practical application. Cycling runs for the photo-oxidation of RhB with 1.0 wt% AuPd/$BiVO_4$ (A-1) was performed to evaluate its photocatalytic stability. After every 25 min of photodegradation process, the sample was recycled by centrifugation, washed with distilled water, and reused in next cycle. Fig. 9 shows that the photocatalytic activity of 1.0 wt% AuPd/$BiVO_4$ still conserve 75% of its original activity after being recycled for four times, which indicates a reliable stability. The photocatalytic stability of 1.0 wt% AuPd/$BiVO_4$ can be even higher when considering the loss of the photocatalyst during the centrifugation process.

3.3. Photocatalytic mechanism discussion

To investigate the photocatalytic mechanism for AuPd/$BiVO_4$ composites, the ESR and SPV techniques were performed. It is generally accepted that organic pollutants can be degraded by photocatalytic oxidation processes. In this procedure, a series of photo-induced reactive species, such as h^+, ·OH, and $\cdot O_2^-$, are suspected to be involved in the photocatalytic degradation reaction. Free radicals in reaction systems are generally detected by means of ESR technique. In ESR test, DMPO (5, 5-dimethyl-1-dimethy-N-oxide) is often used as a radical scavenger, resulting in formation of detectable stable free radicals DMPO-·O_2^- or DMPO-·OH. Fig. 10 shows ESR spectra measured with/without light irradiation over the 1.0 wt% AuPd/$BiVO_4$ photocatalyst with different solvents at room temperature and air atmosphere. No ESR signal can be seen under dark condition. On the contrary, a gradual evolution of ESR peaks for DMPO-·O_2^- adducts (six characteristic peaks, red line) can be observed under visible light irradiation (Fig. 10a). However, no signals of DMPO-·OH adducts were detected both in dark and illuminated conditions (Fig. 10b), which means that $\cdot O_2^-$ is one of the main active species involved in the photodegradation process.

To discover the role of photo-generated holes in the photodegradation process, 0.05 g KI served as scavenger for h^+ and ·OH species was added into the mixed solution, and the same photodegradation of RhB experiment was repeated. It is shown that the degradation activity of 1.0 wt% AuPd/$BiVO_4$ decreased rapidly after addition of KI (Fig. 11), which should be caused by the hole trapping of KI. Therefore, we can conclude that the photo-generated holes are another active species involved in the photodegradation process.

The dynamic behavior of the photo-generated charge carriers was also investigated by using surface photovoltage spectroscopy (SPV) (Fig. 12). Pure $BiVO_4$ nanosheets present a clear positive SPV signal after being excited by light with wavelength ranging from 300 to 525 nm, which is a typical characteristic of n-type semiconductor in SPV. The positive SPV signal indicates that photo-excited positive charges are transferred from inner semiconductor to the surface. The composite samples exhibit stronger SPV signal than pure $BiVO_4$ nanosheets, indicating that the recombination of electron-hole pairs is effectively inhibited. The 1.0 wt% AuPd/$BiVO_4$ sample shows the highest SPV intensity, in turns most efficient

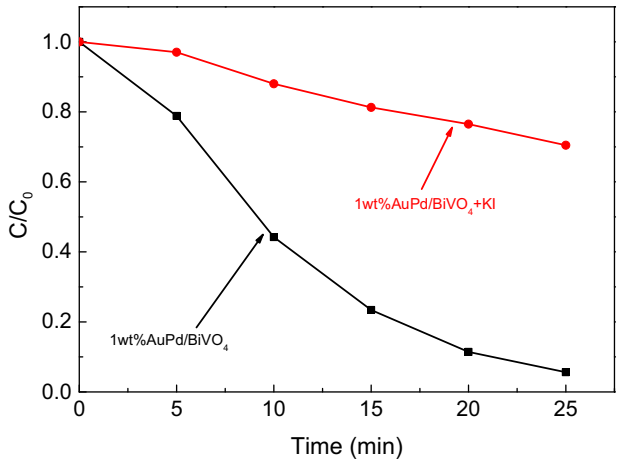

Fig. 11. The photodegradation curves of RhB (black line) and the effect of scavenger KI (red line). (For interpretation of the references to colour in this figure legend, the reader is referred to the web version of this article.)

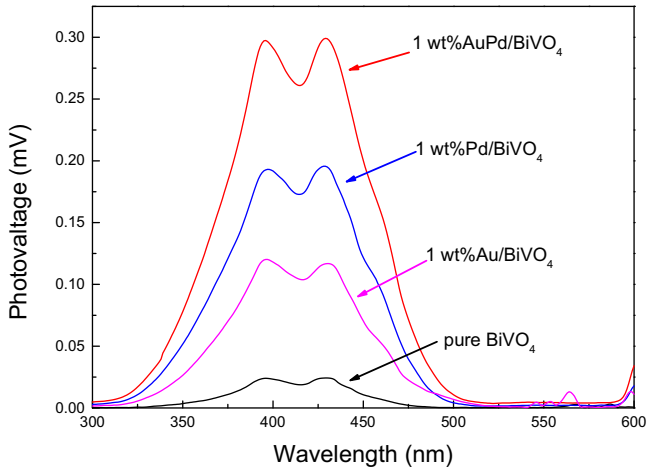

Fig. 12. SPV spectra of the pure $BiVO_4$, 1.0 wt% AuPd/$BiVO_4$, 1.0 wt% Pd/$BiVO_4$ and 1.0 wt% Au/$BiVO_4$.

charge separation efficiency, which is also consistent with the results of photocatalytic experiment and well explained the origin of enhanced catalytic performance in the AuPd/$BiVO_4$ composites. The enhanced separation efficiency of electron-hole pairs can be attributed to the efficient charge transfer at the interface formed between AuPd NPs and $BiVO_4$ nanosheets in the composite samples.

A possible photocatalytic mechanism in AuPd/$BiVO_4$ sample is proposed based on the above observations (as shown in Fig. 13). In general, photo-generated electrons and holes in pristine $BiVO_4$ are likely to recombine after being excited by incident photons. After introducing of AuPd bimetallic NPs, intimate contacts are formed at the AuPd NPs/$BiVO_4$ interfaces and serve as effective channels for the flow of photo-generated charge carriers. As AuPd alloy possesses higher electron-capturing ability due to its low lying of Fermi level, electrons would be stimulated to transfer from $BiVO_4$ to AuPd NPs, results in efficient charge separation efficiency. This improved charge separation efficiency facilitated at the AuPd NPs/$BiVO_4$ interface is the key point responsible for the enhancement of photocatalytic activity. Subsequently, the absorbed O_2 trap electrons to form $\cdot O_2^-$, and holes transfer to the surface of $BiVO_4$. Both $\cdot O_2^-$ and h^+ serve as active species to oxidize organic pollutants so that the as-prepared AuPd/$BiVO_4$ sample exhibit superior photocatalytic activity.

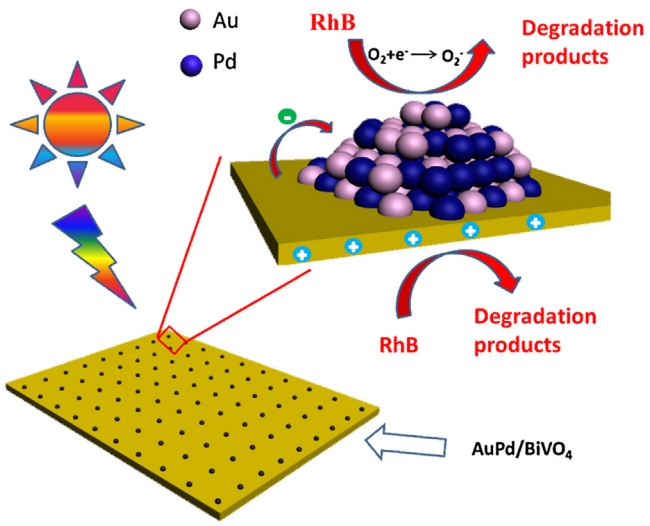

Fig. 13. Schematic diagram illustrating the model of AuPd/$BiVO_4$ production and the proposed degradation mechanism of RhB over AuPd/$BiVO_4$ composites.

4. Conclusions

In summary, novel AuPd bimetallic NPs decorated 2D $BiVO_4$ nanosheets have been successfully synthesized via mild wet-chemical process and facile deposition process. The AuPd NPs dispersed uniformly on the surface of $BiVO_4$ nanosheets and formed intimate interfaces. The 1.0 wt% AuPd/$BiVO_4$ sample exhibited highest activity, which was about 21.9 times higher than pure $BiVO_4$. The enhancement can be attributed to the efficient interfacial charge transfer in the composite sample. The ESR and radical capture experiments confirmed that $\cdot O_2^-$ and h^+ were the active species in the degradation progress. The SPV measurement reveals that decoration of 2D $BiVO_4$ nanosheets with AuPd NPs facilitates charge separation in the composite structure. In conclusion, the AuPd/$BiVO_4$ composites are promising materials in photocatalytic organic degradation process, and our work may provide valuable information for modifying n-type semiconductor photocatalys with improved photocatalytic performance.

Acknowledgements

This work was financially supported by the National Science Foundation of China (Grant No. 21003157, 21273285 and 51572295), Beijing Nova Program (Grant No. 2008B76), and Science Foundation of China University of Petroleum, Beijing (Grant No. KYJJ2012-06-20 and 2462016YXBS05).

References

[1] X.F. Feng, S. Maier, M. Salmeron, J. Am. Chem. Soc. 134 (2012) 5662–5668.
[2] M.R. Hoffmann, S.T. Martin, W. Choi, D.W. Bahnemann, Chem. Rev. 95 (1995) 69–96.
[3] Kudo Y. Miseki, Chem. Soc. Rev. 38 (2009) 253–278.
[4] Y. Zhang, Z.R. Tang, X. Fu, Y.J. Xu, ACS Nano 4 (2010) 7303–7314.
[5] Q. Yu, Z.R. Tang, Y.J. Xu, J. Energy Chem. 23 (2014) 564–574.
[6] S.W. Cao, Z. Yin, J. Barber, F.Y.C. Boey, S.C.J. Loo, C. Xue, ACS Appl. Mater. Interfaces 4 (2012) 418–423.
[7] L. Ge, C.C. Han, J. Liu, Appl. Catal. B: Environ. 108–109 (2011) 100–107.
[8] C.C. Han, L. Ge, C.F. Chen, Y.J. Li, Z. Zhao, X.L. Xiao, Z.L. Li, J.L. Zhang, J. Mater. Chem. A 2 (2014) 12594–12600.
[9] L. Zhang, K.H. Wong, Z. Chen, J.C. Yu, J. Zhao, C. Hu, C.Y. Chan, P.K. Wong, Appl. Catal. A: Gen. 363 (2009) 221–229.
[10] F. Dong, Z.W. Zhao, T. Xiong, Z.L. Ni, W.D. Zhang, Y.J. Sun, W.K. Ho, ACS Appl. Mater. Interfaces 5 (2013) 11392–11401.
[11] Y. Shi, H.Y. Li, L. Wang, W. Shen, H.Z. Chen, ACS Appl. Mater. Interfaces 4 (2012) 4800–4806.
[12] L. Zhang, D. Chen, X. Jiao, J. Phys. Chem. B 110 (2006) 2668–2673.

[13] Y. Sun, B. Qu, Q. Liu, S. Gao, Z. Yan, W. Yan, B. Pan, S. Wei, Y. Xie, Nanoscale 4 (2012) 3761–3767.
[14] L. Zhang, D.R. Chen, X.L. Jiao, J. Phys. Chem. B 110 (2006) 2668–2673.
[15] F.X. Wang, M.W. Shao, L. Cheng, J. Hua, X.W. Wei, Mater. Res. Bull. 44 (2009) 1687–1691.
[16] D.E. Wang, R.G. Li, J. Zhu, J.Y. Shi, J.F. Han, X. Zong, C. Li, J. Phys. Chem. C 116 (2012) 5082–5089.
[17] W.Z. Yin, W.Z. Wang, L. Zhou, S.M. Sun, L. Zhang, J. Hazard. Mater. 173 (2010) 194–199.
[18] M.L. Guan, D.K. Ma, S.W. Hu, Y.J. Chen, S.M. Huang, Inorg. Chem. 50 (2011) 800–805.
[19] L. Ge, Mater. Chem. Phys. 107 (2008) 465–470.
[20] P. Zhang, J.Z. Zhang, Appl. Surf. Sci. 256 (2010) 3224–3227.
[21] W.Z. Wang, X.W. Huang, S. Wu, Y.X. Zhou, L.J. Wang, H.L. Shi, Y.J. Liang, B. Zou, Appl. Catal. B: Environ. 134–135 (2013) 293–301.
[22] S.J. Hong, S. Lee, J.S. Jang, J.S. Lee, Energy Environ. Sci. 4 (2011) 1781–1787.
[23] M. Ou, Q. Zhong, S.L. Zhang, L.M. Yu, J. Alloys Compd. 626 (2015) 401–409.
[24] H.Y. Li, Y.J. Sun, B. Cai, S.Y. Gan, D.X. Han, L. Niu, T.S. Wu, Appl. Catal. B: Environ. 170–171 (2015) 206–214.
[25] C.C. Han, L. Wu, L.E. Ge, Y.J. Li, Z. Zhao, Carbon 92 (2015) 31–40.
[26] N. Zhou, L. Polavarapu, N.Y. Gao, Y.L. Pan, P.Y. Yuan, Q. Wang, Q.H. Xu, Nanoscale 5 (2013) 4236–4241.
[27] Y.Y. Jia, Y.Q. Jiang, J.W. Zhang, L. Zhang, Q.L. Chen, Z.X. Xie, L.S. Zheng, J. Am. Chem. Soc. 136 (2014) 3748–3751.
[28] Z.F. Hu, J.C. Yu, J. Mater. Chem. A 1 (2013) 12221–12228.
[29] L. Kesavan, R. Tiruvalam, M.H.A. Rahim, M.I. bin Saiman, D.I. Enache, R.L. Jenkins, N. Dimitratos, J.A. Lopez-Sanchez, S.H. Taylor, D.W. Knight, C.J. Kiely, G.J. Hutchings, Science 331 (2011) 195–199.
[30] Y.J. Xin, L.E. Wu, L. Ge, C.C. Han, Y.J. Li, S.M. Fang, J. Mater. Chem. A 3 (2015) 8659–8666.
[31] M. Nie, H.L. Tang, Z.D. Wei, S.P. Jiang, P.K. Shen, Electrochem. Commun. 9 (2007) 2375–2379.
[32] R. Su, R. Tiruvalam, Q. He, N. Dimitratos, L. Kesavan, C. Hammond, J.A. Lopez-Sanchez, R. Bechstein, C.J. Kiely, G.J. Hutchings, F. Besenbacher, ACS Nano 6 (2012) 6284–6292.
[33] Y. Lu, J. Zhang, L. Ge, C. Han, P. Qiu, S. Fang, J Colloid Interf. Sci. 483 (2016) 146–153.
[34] M.C. Long, W.M. Cai, J. Cai, B.X. Zhou, X.Y. Chai, Y.H. Wu, J. Phys. Chem. B 110 (2006) 20211–20216.
[35] J. Zhang, H. Cui, B. Wang, C. Li, J.P. Zhai, Q. Li, Chem. Eng. J. 223 (2013) 737–746.
[36] A. Cybula, J.B. Priebe, M.M. Pohl, J.W. Sobczak, M. Schneider, A. Zielińska-Jurek, A. Brückner, A. Zaleska, Appl. Catal. B: Environ. 152–153 (2014) 202–211.
[37] W. Li, Y. Zhang, Y. Bu, Z. Chen, J Alloy. Compd. 680 (2016) 677–684.
[38] F.Q. Zhou, J.C. Fan, Q.J. Xu, Y.L. Min, Appl. Catal. B: Environ. 201 (2017) 77–83.
[39] C. Yu, S. Dong, J. Zhao, X. Han, J. Wang, J. Sun, J Alloy. Compd. 677 (2016) 219–227.
[40] M. Shang, W.Z. Wang, S.M. Sun, J. Ren, L. Zhou, L. Zhang, J. Phys. Chem. C 113 (2009) 20228–20233.